NJC

PAPER

View Article Online
View Journal

Cite this: DOI: 10.1039/c5nj02748a

Catalytic activity of silicon carbide nanotubes and nanosheets for oxidation of CO: a DFT study†

Parisa Nematollahi and Mehdi D. Esrafili*

Received (in Montpellier, France) 11th October 2015,
Accepted 13th January 2016

DOI: 10.1039/c5nj02748a

www.rsc.org/njc

As is well-known, searching for an efficient catalyst that can oxidize CO molecules is of great importance in the removal of this poisonous gas. Using density functional theory calculations, we report the oxidation of CO by molecular O_2 on a finite-sized silicon carbide nanotube (SiCNT) and nanosheet (SiCNS). Both Eley–Rideal (ER) and Langmuir–Hinshelwood (LH) oxidation mechanisms are considered. The CO oxidation by O_2 on SiCNT and SiCNS surfaces occurs *via* a two-step mechanism: (1) $O_2 + CO \rightarrow OOCO \rightarrow O_{ads} + CO_2$ and (2) $O_{ads} + CO \rightarrow OCO \rightarrow CO_2$, proceeding *via* LH and ER mechanisms, respectively. The activation energies of these two steps over the SiCNT (SiCNS) are 0.86 (0.27) and 0.97 (0.12) eV, respectively. Results indicate that the CO oxidation over the SiCNS is more favorable than that over the SiCNT, due to its lower energy barriers. In addition, the increasing of the tube length and curvature effects on the adsorption of an O_2/CO molecule is also studied. This study has useful guidance for fabricating SiCNTs and SiCNSs for CO oxidation with high activity properties.

1. Introduction

The oxidation of carbon monoxide (CO) has been attracting considerable research interest for many years.[1] This gas molecule is highly toxic to human beings and animals, because it inhibits the consumption of oxygen by body tissues. Moreover, it is colorless, odorless, and tasteless, thus, human beings do not have timely alertness to its presence.[2] Therefore, the oxidation of CO to carbon dioxide (CO_2) has attracted extensive research interest due to its importance in applications such as cleaning air, reducing CO emissions from automobiles and industries,[3–5] and CO removal from hydrogen gas fuels to avoid electrode poisoning in fuel cells.[6] Many scientists have investigated the oxidation of CO by various noble metals such as Pd–Au,[7] Ag,[8] Pd,[9] Pt, and Rh.[10,11] The high activity and selectivity of these noble metal catalysts for many chemical reactions make them important materials, which can be widely used in industry. They have high surface area and can be dispersed finely on a support. Furthermore, they can be effectively used for catalytically active components. However, the high cost, scarcity and high reaction temperature for efficient operation of these noble metal catalysts hinder their usage on a large scale. Therefore, the development of either low-cost alternatives or catalysts with higher activity for oxidation of CO is desirable.

In recent years, two-dimensional nanomaterials such as a graphene sheet with one-atom-thick carbon honeycomb structure have attracted considerable attention because of their intrinsic properties and potential usage in nanoelectronics.[12–19] It should be noted that the future application of graphene-based catalysts is majorly inhibited, because pristine graphene is chemically rather inert due to the existence of strong π bonding between sp^2 carbon atoms, so that the interaction between graphene and the reaction center is rather weak.[19,20] Chemical doping by incorporation of heteroatoms, such as B, N and Si, into the sp^2-hybridized carbon framework of graphene is a promising and feasible way to modify its chemical reactivity and surface properties.[21–23] Although C and Si are both in the fourth row of the periodic table and have the same number of valence electrons, they show different bonding characteristics. This occurs due to the different hybridization of C (sp^2) and Si (sp^3) atoms, which leads to the formation of linear chains and planar structures in contrast to three-dimensional materials, respectively.[24] The development of silicon carbide (SiC) technology over the last few years has been quite impressive, with significant improvements in technology, materials processing, electronic devices and sensors. The underlying motivation for the investments in SiC technology is the excellent material properties, which are mainly originated from the strong Si–C bonds. In fact, SiC exists in a large number of different crystalline structures built from the same Si–C subunit organized into a variety of stacking sequences.[25] Such polytypes are identified by the type of crystal lattice (*i.e.* hexagonal, cubic, or rhombohedral) and the number of layers making up the repeat pattern, *e.g.* 4H–SiC has a hexagonal lattice with a four-layer repeat structure. Among the approximately 250 known SiC polytypes, the majority of research studies and developments have focused on only three, *i.e.* 3C,

Laboratory of Theoretical Chemistry, Department of Chemistry, University of Maragheh, P.O. Box: 5513864596, Maragheh, Iran.
E-mail: esrafili@maragheh.ac.ir; Fax: (+98) 4212276060; Tel: (+98) 4212237955

† Electronic supplementary information (ESI) available. See DOI: 10.1039/c5nj02748a

6H and 4H, in which the 4H polytype is the most common for electronic devices and sensors. In general, SiC has a unique combination of high critical field and high thermal conductivity. In comparison with other pristine and doped carbon materials, SiC with the atom ratio of 1 : 1 provides more active reaction sites for the adsorption of gas molecules. For example, Virojanadara and Johansson[26] studied the oxygen adsorption at different temperatures on the SiC(0001) surface using photoemission. Chang *et al.*[27] performed first-principles calculations to explore the physical origin of hydrogen-induced semiconductor surface metallization observed in the β-SiC(001)-3 × 2 surface. They showed that the surface metallization arises from a novel mechanism of n-type doping of the surface band *via* formation of hydrogen bridge bonds (*i.e.*, Si–H–Si complex). The hydrogen strengthens the weak Si–Si dimers in the subsurface by forming hydrogen bridge bonds and donates an electron to the surface conduction band.

Comparing the relative stability of layered and cubic SiC sheets (with layer number, N) in the oxygen reduction reaction (ORR) showed that the former SiC is energetically more favorable than the latter when $N < 4$, whereas the cubic form is more stable when $N \geq 4$.[28] However, despite the weak layer-layer interaction in the SiC layered sheet, its structure is still stronger than that of the cubic SiC sheet when $N < 4$. This claim was also proved experimentally recently, which indicates that the thickness of a synthesized two-dimensional SiC nanosheet (SiCNS) is in the range of 0.5–1.5 nm.[29] Wang[30] studied the adsorption of an HCOH molecule on the SiC sheet. They found that the C atom of the SiC sheet is the active adsorption site and the HCOH molecule prefers the C atom rather than the O and H atoms close to the SiC sheet. On the other hand, Gori *et al.*[31] proposed that the replacement of half of the C atoms by Si atoms opens a large direct electronic gap. This effect makes functionalized SiC layers very interesting for electronic applications, *e.g.*, as electron or hole filters. Recently, there have been great efforts to study the potential applications of SiC nanotubes (SiCNTs) both theoretically and experimentally. SiCNTs are analogues of carbon nanotubes (CNTs), which have been experimentally synthesized from the reaction of SiO and multi-walled CNTs.[32] In SiCNTs, carbon and silicon atoms exist in a 1 : 1 ratio. Moreover, because of their unique structural properties, gas molecules can bind to the side walls of these nanotubes with larger binding energies than those bound to CNTs.[24] For instance, Gao *et al.*[33] found that NO and N_2O molecules can be chemisorbed on SiCNTs, while this is not the case for CNTs. In addition, Wu *et al.*[34] studied the interaction between two toxic gases (CO and HCN) on SiCNTs and found that SiCNTs exhibit better reactivity toward these adsorbates than CNTs. SiCNTs have semiconductor properties regardless of their chirality or diameter.[35,36] Moreover, due to the significant charge separation between the silicon and carbon atoms in SiCNTs, the silicon atom (electron-deficient) and carbon atom (electron-rich) can be viewed as a Lewis acid and base, respectively. This provides more active reaction sites than the amount present in CNTs or doped carbon materials, which allow SiCNTs to serve as feasible metal-free catalysts.[37–40]

In this study, by density functional theory (DFT) calculations, we present the oxidation of CO by molecular O_2 on a finite-sized zigzag (6,0) SiCNT. The optimized structures and adsorption energies for the interaction of O_2 and CO molecules with the SiCNT surface are discussed in detail. The energy barrier for each elementary step in the CO oxidation reaction is obtained, and the corresponding mechanisms are explained *via* the electronic structures. Moreover, we estimate that a layered SiC sheet can exhibit outstanding catalytic activity for CO oxidation, which makes it a favorable candidate for the next generation of catalysts for oxidation/reduction of harmful gases. To the best of our knowledge, no prior theoretical investigation has been reported on this issue.

2. Computational details

All DFT calculations were performed using the Gaussian 09 package.[41] The use of the M06-2X density functional is known as a reliable method for studying non-covalent interactions; therefore, we preferred to apply this method for our calculations. M06-2X is a global hybrid meta-GGA functional, with 54% HF exchange, for top-level across-the-board performances in all areas of chemistry. There are many studies that indicate that M06-2X can yield excellent results in calculating main group thermochemistry parameters and barrier heights over the most popular DFT methods, *e.g.* B3LYP.[42,43] Therefore, the structure of each monomer and complex was fully optimized at the M06-2X/6-31G* computational level. Frequency calculations at the same level were carried out to confirm that the structures obtained corresponded to energy minima. The CO oxidation reaction was carried out over a truncated (6,0) SiCNT with 24 Si and 24 C atoms, which was used as the basic model for the calculations. To investigate the curvature effect, these mechanisms were also studied over the (5,0) SiCNT in detail. To avoid boundary effects, both ends of the truncated (6,0) and (5,0) SiCNTs were capped with hydrogen atoms to saturate dangling bonds. Both the singlet and triplet spin states were considered for molecular oxygen adsorption. Moreover, an elongated (6,0) SiCNT with a length of about 17 Å was used to study the effect of increasing the length on the O_2/CO adsorption on (6,0) SiCNT. For studying the oxidation of CO over a SiCNS, a flatten SiC monolayer containing 46 Si and C atoms were constructed, with the ending atoms saturated by H atoms. The adsorption energy (E_{ads}) of adsorbate was calculated based on the equation as follows:

$$E_{ads}(A) = E_{A-M} - E_M - E_A \quad (1)$$

where E_{A-M}, E_M and E_A are the total energy of the adsorbate-substrate system, that of the substrate, and the energy of the adsorbate in the gas phase, respectively.

3. Results and discussion

3.1 Adsorption of O_2 on the SiCNT and SiCNS

As is clear from Fig. 1 that a finite-sized zigzag (6,0) SiCNT consists of alternating C and Si atoms with two types of Si–C bonds: one has a bond length of 1.84 Å and is in parallel with the tube axis (named A bond), and the other has a bond length

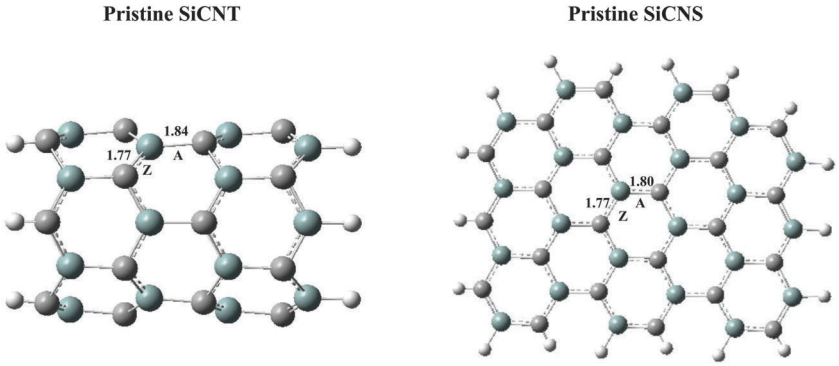

Fig. 1 Optimized structures of pristine (6,0) SiCNT and SiCNS. All bond distances are in Å.

of 1.77 Å and zigzags across the tube axis (named Z bond). The average calculated Si–C bond distances are generally in good agreement with previous reports.[44,45] The Mulliken charge density analysis indicates that about 0.6 electrons are transferred from the Si atom to its nearest carbon atoms, which is much more than that of boron nitride nanotubes.[37] Our results indicate that the (6,0) SiCNT has a band gap of 1.52 eV, consistent with the 1.42 eV reported by Wang and Liew.[46] On the other hand, one can observe from Fig. 1 that the calculated Si–C bond lengths in a SiC monolayer are 1.77 (Z bond) and 1.80 Å (A bond), which are smaller than those of the β-SiC crystal structure (1.89 Å),[47] but in good agreement with previous studies.[30,45,48,49] This supports the choice of computational method. Analogous with that of the SiCNT, a net charge of about 0.6 *e* is transferred from a Si atom to the adjacent C atoms of the sheet. Therefore, it can be proposed that the positive Si (electron-deficient) and negative C (electron-rich) atoms of the SiCNT/SiCNS can be viewed as a Lewis acid and base, respectively.

To study the O_2 adsorption on the SiCNT, we start with the cylindrical structure of the pristine (6,0) SiCNT. To study the CO oxidation by molecular O_2, the adsorption of O_2 and CO molecules over the SiCNT surface should first be considered. To achieve this purpose, different probable orientations of these gas molecules are tested to find the most energetically stable configurations. For O_2 adsorption, both triplet and singlet spin states are considered. For the adsorption of an O_2 molecule in its triplet ground state, two possible configurations of adsorbed O_2 over a SiCNT (O_2–SiCNT) are obtained, which are depicted in Fig. 2. The corresponding adsorption energies (E_{ads}) along with geometric and thermodynamic quantities, such as binding distances (R), Gibbs free energy change (ΔG_{298}), enthalpy change (ΔH_{298}) and charge transfer (q_{CT}), are listed in Table 1. According to previous studies,[50–52] there are two common adsorption configurations for triplet O_2 in which the O_2 molecule is placed in two directions, *i.e.* parallel (side-on) and perpendicular (end-on). In the chemisorbed configuration **A**, one of the oxygen atoms of O_2 approaches the Si atom of the SiCNT in parallel position with E_{ads} value of −1.01 eV and Si–O bond length of 1.75 Å (Table 1). The consideration of counterpoise correction for the basis set superposition error (BSSE) decreases the adsorption energy of this complex by 0.16 eV. These results indicate that there is a significant interaction between the O_2 molecule and the tube surface, which is in the range of chemisorption. This value is a little larger than that in a Si-doped boron nitride nanosheet and nanotube (1.73 Å),[51] but is smaller than those obtained for (8,0) SiCNT.[53] Moreover, the Si atom of the SiCNT, which is bonded to the O atom in this chemisorption configuration, is slightly pulled out of the sidewall and therefore the three corresponding Si–C bonds are slightly elongated. According to thermochemical results, the adsorption process to form complex **A** is an exothermic reaction, with ΔH_{298} and ΔG_{298} values of −1.04 and −0.62 eV, respectively (Table 1).

The physisorbed configuration **B** with the negligible E_{ads} of −0.19 eV and large Si–O bond length (2.90 Å) indicates a weak interaction of molecular O_2 with the tube surface. Moreover, it can be concluded from the thermochemical results that the formation of this complex is exothermic (ΔH_{298} = −0.15 eV), but it cannot be easily performed at room temperature (Table 1). Thus, it can be concluded from Table 1 results that between these two configurations for triplet O_2 adsorption, complex **A** is the more energetically stable configuration for CO oxidation. On the other hand, the optimized structures of singlet O_2 adsorption over SiCNT with their bond length values are displayed in Fig. S1 of ESI.† There are two different adsorption configurations (**C** and **D**) in which the singlet O_2 reacts with SiCNT and forms two stable [2+2]-cycloaddition products. In both configurations, the O_2 molecule prefers to form two bonds with the Si and C atoms of the SiCNT, whereas the O–O bond is placed parallel to the surface (Fig. S1, ESI†). We note that the same configurations were also obtained in a previous study by Szabó *et al.*[54] Moreover, these results are consistent with the findings of Cao *et al.*,[53] in which singlet O_2 adsorption on the tube surface can yield cycloaddition structures with large adsorption energy and sizable charge transfer. The corresponding adsorption energies for complexes **C** and **D** are calculated to be about −2.09 and −3.16 eV, respectively, which are larger (more negative) than those of triplet O_2. However, our DFT calculations reveal that the adsorption configuration for the singlet O_2 state has the higher (less negative) total energy compared to that of the triplet state. The energy difference between the triplet and singlet states of O_2 adsorption is calculated to be about 0.4 eV, which confirms

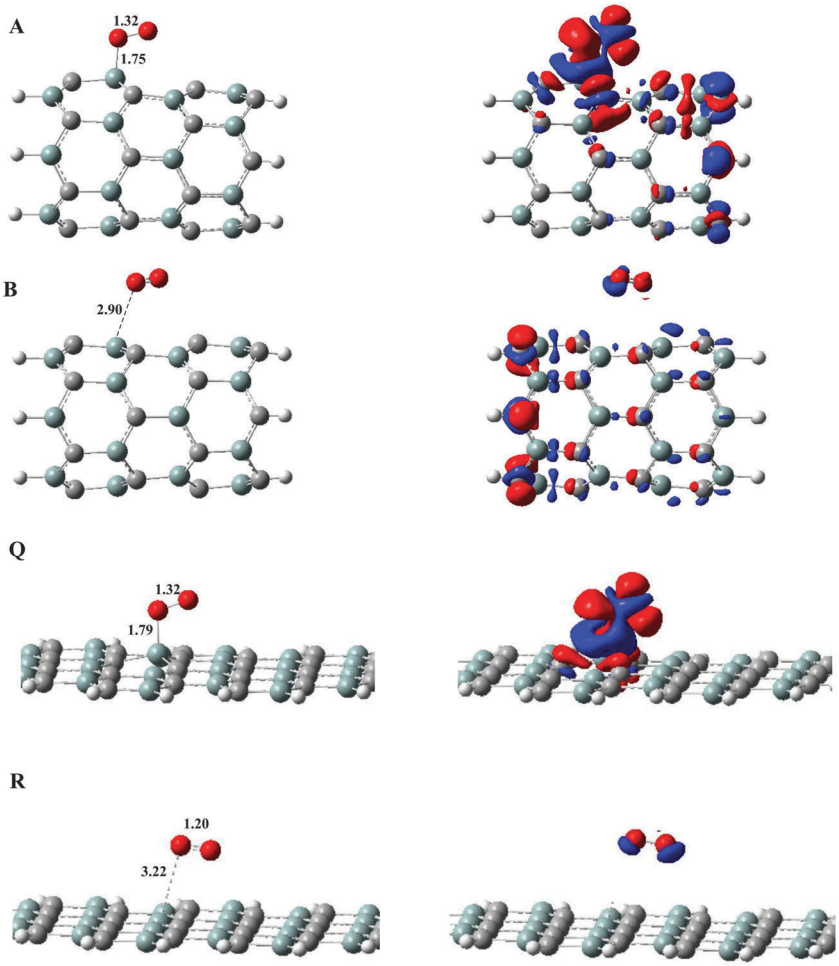

Fig. 2 Optimized structures of adsorbed O_2 (triplet) over (6,0) SiCNT and SiCNS with their electron density difference (EDD) maps (±0.001 au). In the EDD maps, the charge depletion and accumulation sites are displayed in red and blue, respectively. All bond distances are in Å.

Table 1 Calculated binding distances (R), adsorption energy (E_{ads}), Mulliken charge-transfer values (q_{CT}), change of Gibbs free energy (ΔG_{298}) and change of enthalpy (ΔH_{298}) of the adsorbed triplet O_2– (complexes **A** and **B**), CO– (complexes **E** and **F**) over (6,0) SiCNT, triplet O_2– (complexes **Q** and **R**), and CO– (complexes **S** and **T**) on SiCNS

Surface	Configuration	R (Å)	E_{ads} (eV)	q_{CT} (e)	ΔG_{298} (eV)	ΔH_{298} (eV)
SiCNT	**A**	1.75	−1.01	0.86	−0.62	−1.04
	B	2.90	−0.19	0.03	0.14	−0.15
	E	2.16	−0.38	0.16	0.06	−0.33
	F	2.89	−0.20	0.04	0.17	−0.16
SiCNS	**Q**	1.79	−0.20	0.50	0.40	−0.13
	R	3.22	−0.14	0.03	0.25	−0.14
	S	1.98	−0.18	0.20	0.24	−0.14
	T	3.24	−0.07	0.04	0.32	−0.04

that a chemisorbed O_2 molecule at the triplet state is more stable than that at the singlet state. This can also be supported from other theoretical investigations.[53]

In addition, in complex **A**, a large net charge of 0.86 e is transferred from the SiCNT to the $2\pi^*$ orbital of the O_2 molecule, which leads to the elongation of the O–O bond from 1.20 Å in the gas phase to 1.32 Å in the adsorbed complex. This indicates that the reactivity of the O_2 molecule increases upon its adsorption over the SiCNT surface. These results are confirmed by the electron density difference (EDD) map, which is shown in Fig. 2. In the EDD map, the charge depletion and accumulation sites are displayed in red and blue, respectively. As is clear, strong charge depletion and accumulation are observed at the O–O and around the Si–O bond, respectively, which confirms the strong chemical adsorption of the O_2 molecule with the surface. In contrast to that in complex **A**, in complex **B**, a negligible charge of 0.03 e is transferred from the O_2 molecule to the tube surface, which shows that there is a weak interaction between the gas molecule and the surface. Moreover, the EDD maps of configurations **C** and **D** (Fig. S1, ESI†) with a great charge transferring (Table S1, ESI†) show a sizable charge accumulation around the Si–O and C–O bonds, which are caused by the strong interaction of the O_2 molecule with the SiCNT surface.

Furthermore, it was interesting to study the length effect of the (6,0) SiCNT on the adsorption of the O_2 molecule (Fig. S2, ESI†). The interaction of the O_2 molecule with the large-length (6,0) SiCNT is studied by performing a single point energy calculation for the most stable configuration of the O_2–SiCNT

(configuration **A**), named complex **G**. As a result, the E_{ads} of the O_2 molecule increases to −1.39 eV, while the Si–O bond length is about 1.75 Å (Table S1, ESI†). It is found that there is not a significant difference between the O_2 adsorption over large-length and short-length (6,0) SiCNT. Therefore, to facilitate the calculations, the short-length nanotube is used as a support to study the CO oxidation mechanisms.

Along with these oxidation mechanisms, another question arises of whether the adsorption of O_2 depends on the diameter size of the nanotube. To find the answer to this question, the curvature effect on the adsorption of an O_2 molecule over a (5,0) SiCNT is investigated carefully. Fig. S3 of ESI,† indicates the most stable adsorption configurations of the O_2 molecule over the (5,0) SiCNT with their corresponding bond length values. Both the triplet and singlet spin states of the O_2 molecule are also considered over (5,0) SiCNT (complexes **I**, **K** and **L**). Moreover, the geometric and thermodynamic parameters are listed in Table S2 (ESI†). Comparing the E_{ads} of O_2 over (6,0) and (5,0) SiCNTs shows that the adsorption energy of the triplet O_2 is increased with the reduction of tube diameter because of the curvature effect (Table S2, ESI†). This can be attributed to the enhanced sp^3-hybridization of the surface Si atoms. As the tube diameter decreases, more π electrons of the tube go out of the surface plane, and this facilitates the sp^3-hybridization of the surface Si atoms, which helps the adsorption reaction of O_2 over the SiCNT.

Furthermore, we studied the probable adsorption configurations for O_2 adsorption over SiCNS. According to the previous discussion about different spin states of an O_2 molecule, because the triplet spin state of this gas molecule is more stable than the singlet state, herein, the triplet state is considered for adsorbed O_2 configurations. There are two possible adsorption configurations in which the O_2 molecule is chemically (complex **Q**) or physically (complex **R**) adsorbed to the surface, which are shown in Fig. 2. Moreover, the geometric and thermodynamic parameters of these complexes are reported in Table 1. Analogous with that for the complex **A**, the preferred configuration for O_2 adsorption on the SiCNS (complex **Q**) is formed when one of its oxygen atoms binds to the Si atom of the surface with Si–O distance of 1.79 Å, which is a little larger than that reported by Zhang *et al.*[28] The calculated E_{ads} is about −0.20 eV, which is significantly lower than that in its tubular form. According to Table 1 results, there is about 0.5 *e* charge transfer from the SiCNS to the O_2 molecule, occupying its $2\pi^*$ orbitals, resulting in the O–O bond elongation to 1.32 Å, which is a typical value of peroxo species. This can also be observed from its EDD isosurface in Fig. 2 in which a sizable charge density is accumulated around the Si–O bond length, which confirms the chemical binding. For the complex **R**, as shown in Fig. 2, the physisorbed O_2 molecule with Si–O distance of 3.22 Å has the same adsorption energy as complex **Q** (Table 1). The negligible charge transfer (0.03 *e*) from the surface to O_2 molecule is determined by the EDD map, which indicates that there is no considerable interaction between the molecular O_2 and the SiCNS. Thus, it can be proposed that the chemisorbed configuration is more favorable for the CO oxidation reaction. It should be noted that the formation of both configurations are exothermic, but they cannot be feasibly performed at room temperature (Table 1).

3.2 Adsorption of CO on the SiCNT and SiCNS

Analogous with O_2 adsorption, different possible adsorption geometries were considered to find the most stable configurations of a single CO molecule adsorbed on the SiCNT surface. According to previous studies,[34,55] there are two different configurations for the CO adsorption over SiCNTs, in which the CO molecule is adsorbed with either the C or O atom on the Si atom of the tube surface (Fig. 3).

Comparing the E_{ads} of these two configurations, which are listed in Table 1, demonstrates that the most favorable configuration of the CO molecule is achieved on top of a Si atom at an end-on direction. In this configuration, the CO molecule adsorbs *via* its C atom by the Si atom of SiCNT and forms configuration **E** with the E_{ads} and Si–C_{CO} bond length of −0.38 eV and 2.16 Å, respectively. This is close to CO adsorption values over (7,0) SiCNT[56] and is larger than that over Fe-[57] and Si-embedded graphene.[22] The small E_{ads} and long distance of the CO molecule from the tube surface show that the physisorbed CO molecule is not strong enough to prevent desorption at room temperature. The formation process of complex **E** is exothermic (ΔH_{298} = −0.33 eV), but the positive magnitude of ΔG_{298} (0.06 eV) indicates that this complex would be thermodynamically unstable in the gas phase at 298 K. In configuration **F**, the CO molecule is weakly adsorbed *via* its O atom to the Si atom in a tilted position with the SiCNT surface (E_{ads} = −0.20 eV and Si–O = 2.89 Å). Similar to complex **E**, this configuration is achieved *via* an exothermic reaction with ΔH_{298} value of about −0.16 eV, and it is thermodynamically feasible at room temperature (Table 1). Thus, it is concluded that complex **E** should be chosen as the most stable configuration for studying the CO oxidation reaction mechanism due to its larger (more negative) E_{ads} and thermochemical values (Table 1).

According to Table 1, the net charge transfer values of configurations **E** and **F** are about 0.16 and 0.04 *e*, respectively, which are transferred from the CO molecule to the SiCNT surface. The EDD isosurfaces in Fig. 2 also indicate that during the CO adsorption, some electron density shifts from the CO molecule to the SiCNT surface. In addition, there is not a considerable charge accumulation around the Si–C_{CO} and Si–O bonds, which confirms the weak interaction between the gas molecule and the SiCNT. It is important to know that the amount of electron density redistribution in the CO adsorption configurations is smaller than those of O_2. Therefore, this result points out that during the adsorption process, the CO molecule becomes less activated than the O_2 molecule.

Studying the length effect of the (6,0) SiCNT on the adsorption of a CO molecule (configuration **H**) using a single point calculation shows an increase in the E_{ads} and Si–O bond length of the CO molecule (see Table S1 and Fig. S2, ESI†). Moreover, investigating the curvature effect on the CO adsorption over the (5,0) SiCNT demonstrates that in comparison with the complex **E**, the adsorption energy of complex **J** is increased

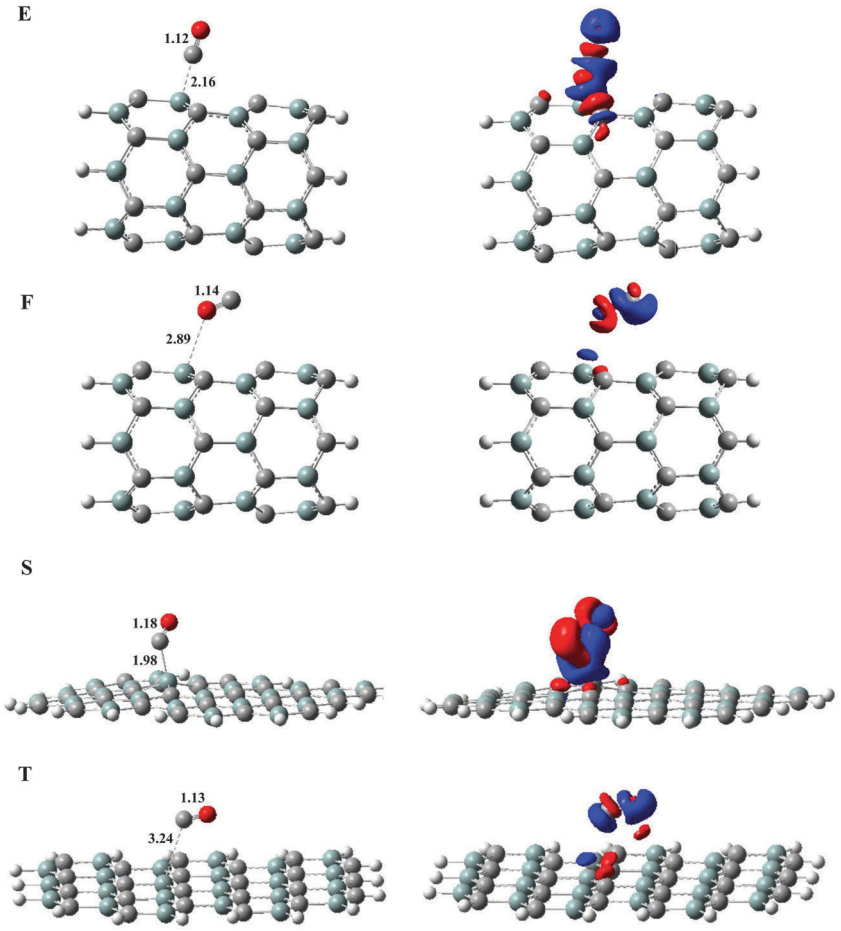

Fig. 3 Optimized structures and computed EDD isosurfaces (±0.001 au) of CO adsorption over the (6,0) SiCNT and SiCNS. In the EDD maps, the charge depletion and accumulation sites are displayed in red and blue, respectively. All bond distances are in Å.

with the reduction of the tube diameter due to the curvature effect (Table S2, ESI†).

There are two physically (complexes **S** and **T**) adsorbed configurations for the adsorption of a CO molecule over a SiCNS surface (Fig. 3). The main preferred configuration for CO adsorption (complex **S**) is achieved when the C atom of CO binds to the Si atom while its O atom is away from the surface. The Si–C_{CO} bond length is about 1.98 Å, which confirms that the CO is physically adsorbed over the SiCNS (Table 1). This weak interaction between Si and C leads to the smaller E_{ads} value (−0.18 eV) than that in SiCNT. In addition, it can be estimated that a small net charge (0.20 *e*) is transferred from the CO molecule to the SiCNS. This is acceptable because of the far distance between the C_{CO} and Si atoms. The EDD map of this configuration also confirms that there is no considerable charge density accumulation and therefore no chemical binding between the C_{CO}/Si atoms. In complex **T**, the binding distance between the CO molecule and Si atom of the surface increases to 3.24 Å. The unchanged C═O bond length compared with its value in the gas form (1.13 Å) shows that there is no strong interaction and therefore no charge transfer between the C atom of the molecular CO and Si atom of the SiCNS (Fig. 3). It is noticeable that both CO-adsorbed configurations over SiCNS are produced *via* an exothermic reaction ($\Delta H_{298} < 0$), but these processes cannot occur at ambient conditions ($\Delta G_{298} > 0$).

In general speaking, comparing CO and O_2 adsorption configurations over both SiCNT and SiCNS surfaces indicates that the O_2 adsorption over the SiCNT surface changes its electronic structure properties more significantly than CO adsorption due to the larger E_{ads} and charge-transfer. In addition, according to our findings, a chemisorbed O_2 molecule with a triplet state is more stable than a singlet one. Thus, it can be suggested that when an O_2/CO mixture is injected as the reactant gas, the Si atoms of the SiCNT should be covered by triplet O_2 molecules. On the other hand, studying the O_2/CO adsorption configurations over the SiCNS shows that in comparison with SiCNT, molecular O_2 is weakly adsorbed over the SiCNS. Despite the fact that O_2 is weakly activated over the SiCNS, in the following section, we consider the CO oxidation reaction on both surfaces.

3.3 CO oxidation reaction on the SiCNT and SiCNS

There are two established mechanisms for the CO oxidation reaction, namely, the Eley–Rideal (ER) and Langmuir–Hinshelwood (LH) mechanisms.[50] In the ER mechanism, the gas-phase CO molecule approaches the activated O_2, but in the LH mechanism

the co-adsorption of CO and O_2 molecules occurs before the reaction. Actually, the right pathway on the catalyst is determined by the adsorption ability of the gas molecule. Previous studies have suggested that the exact reaction pathway is related to the special catalyst that is used. For example, Nigam and Majumder[58] indicated that CO oxidation on Fe clusters encapsulated by a BN nanocage cannot be initiated *via* the LH mechanism, whereas LH reaction was the starting point for CO oxidation on Cu- and Au-doped graphene.[50,59] Li *et al.*[57] proposed that Fe-doped graphene is a favorable catalyst for CO oxidation through the ER mechanism. In addition, as discussed above, because the adsorption energy (E_{ads}) of the O_2 molecule is larger than that of CO, the O_2 molecule is expected to preferentially occupy the Si sites and is activated by interaction with the Si atom of the SiCNT. Therefore, the question of which mechanism is the most favorable for the CO oxidation reaction over SiCNT (ER or LH) may arise. To find the answer to this question, the minimum energy pathway (MEP) with the optimized structures for the initial state (IS), transition state (TS) and final state (FS) of the CO oxidation reaction is calculated, in which both ER and LH mechanisms are considered (Fig. 4). Moreover, the corresponding activation energies (E_{act}) and thermodynamic parameters are listed in Table 2. It should be noted that in comparison with the LH mechanism, the oxidation of CO by molecular O_2 has a high energy barrier when it proceeds *via* the ER mechanism. Moreover, the reactivity of the surface is so high that it prevents the CO molecule from reacting with the O_2 molecule directly. Thus, it can be concluded that the LH mechanism is the most probable mechanism for CO oxidation over a SiCNT according to the reaction

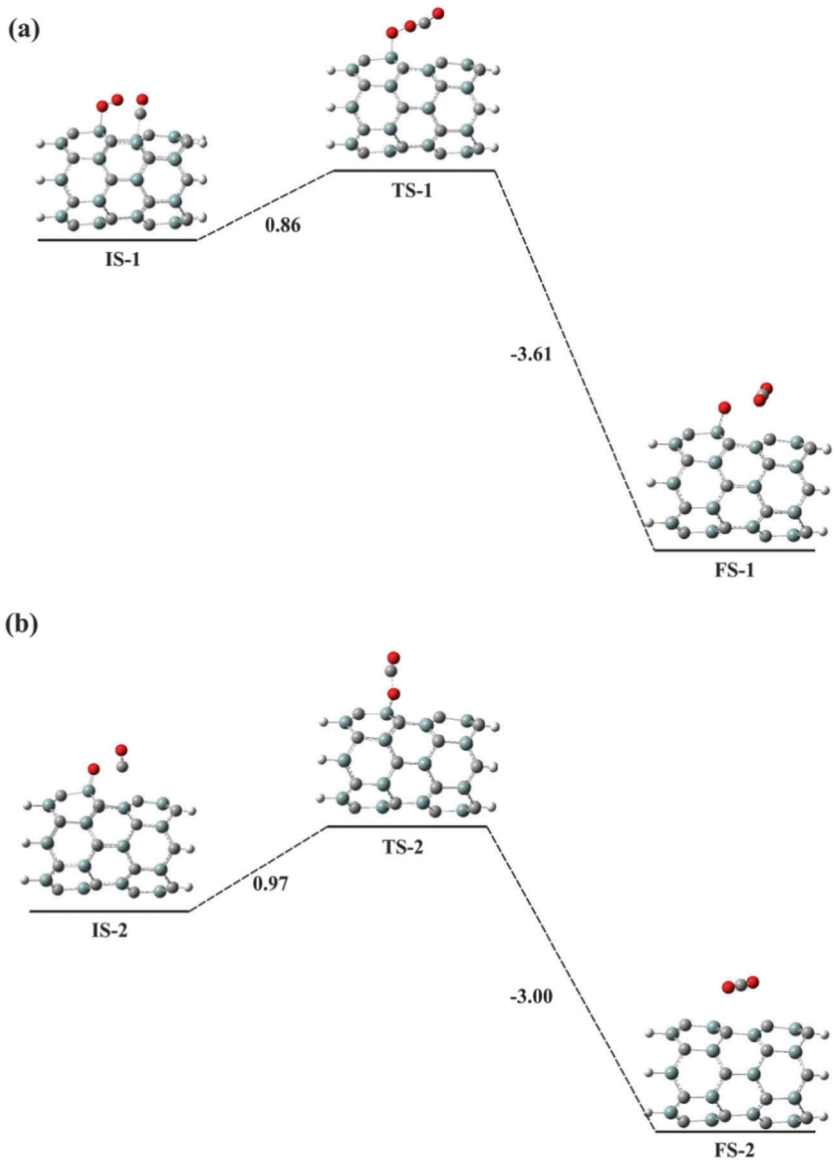

Fig. 4 Schematic energy profile corresponding to local configurations along the (a) $O_2 + CO \rightarrow O_{ads} + CO_2$ and (b) $O_{ads} + CO \rightarrow CO_2$ reaction paths. All energies are in eV.

Table 2 Calculated activation energy (E_{act}), reaction energy (ΔE), change of Gibbs free energy (ΔG_{298}) and enthalpy (ΔH_{298}) for different pathways of CO oxidation over SiCNT and SiCNS

Reaction	E_{act} (eV)	ΔE (eV)	ΔG_{298} (eV)	ΔH_{298} (eV)
(6,0) SiCNT				
IS-1 → FS-1	0.86	−2.75	−2.79	−2.75
IS-2 → FS-2	0.97	−2.03	−1.98	−2.03
SiCNS				
IS-5 → FS-5	0.27	−2.78	−2.72	−2.78
IS-6 → FS-6	0.12	−1.32	−1.34	−1.32

pathway $O_2 + CO \rightarrow O_{ads} + CO_2$ as a starting point, which is followed by an ER mechanism *via* the $O_{ads} + CO \rightarrow CO_2$ reaction.

As mentioned above, the CO oxidation mechanism over a (6,0) SiCNT starts with complex **A** due to the strong interaction of its O_2 molecule with the tube surface, which is an exothermic process with E_{ads} ($CO + O_2$) = −2.14 eV, larger than the sum of the individual E_{ads} values of CO and O_2 (see Table 1). To reach the IS-1, all the probable adsorption sites were checked to find the most stable configuration for a co-adsorbed $O_2 + CO$ system (Fig. S4, ESI†). Among them the most stable co-adsorbed configuration was selected as the initial state (IS-1), in which CO and O_2 in this configuration are perpendicular and parallel to the SiCNT surface, respectively (Fig. 5). In IS-1, after the CO molecule approaches the activated O_2, the O–O bond is slightly elongated to the CO–O_2 distance of 2.7 Å. Then, the carbon atom of CO gets closer to the O_2 molecule to reach the TS-1. Thus, a peroxo-type O–O–C–O complex is formed over the SiCNT surface in which the bond lengths of O_2 and CO are elongated to 1.37 and 1.14 Å, respectively, which are close to the values for the reaction of CO with O_2 over Si-embedded graphene.[22] The corresponding energy barrier of TS-1 along the reaction pathway is 0.86 eV (Fig. 4), which can be compared with that of similar theoretical studies on different surfaces such as Sn-,[60] Fe-[57] or Si-embedded graphene.[22] Passing over TS-1, the Si–O bond length decreases from 1.72 to 1.68 Å until the FS-1 state is reached and $CO_2 + O_{ads}$ is formed over the tube surface. Then, the physisorbed CO_2 molecule is released from the SiCNT surface easily. The reaction pathway IS-1 → FS-1 is exothermic with ΔH_{298} = −2.75 eV and is thermodynamically feasible at ambient conditions (ΔG_{298} = −2.79 eV).

We have also investigated whether the ER or LH mechanism in the second step is possible after the production of the first CO_2 molecule. In this step, the CO molecule is oxidized by the remaining O_{ads} after the first step. Calculated results show that the LH mechanism in this step proceeds with great difficulty and is almost impossible. Therefore, we study the favorable reaction processes in this step through the ER mechanism. Similar to IS-1, when the CO molecule approaches O_{ads}, different configurations are formed as the IS-2 (Fig. S4 of ESI†), and among them the most stable configuration is chosen as the starting point.

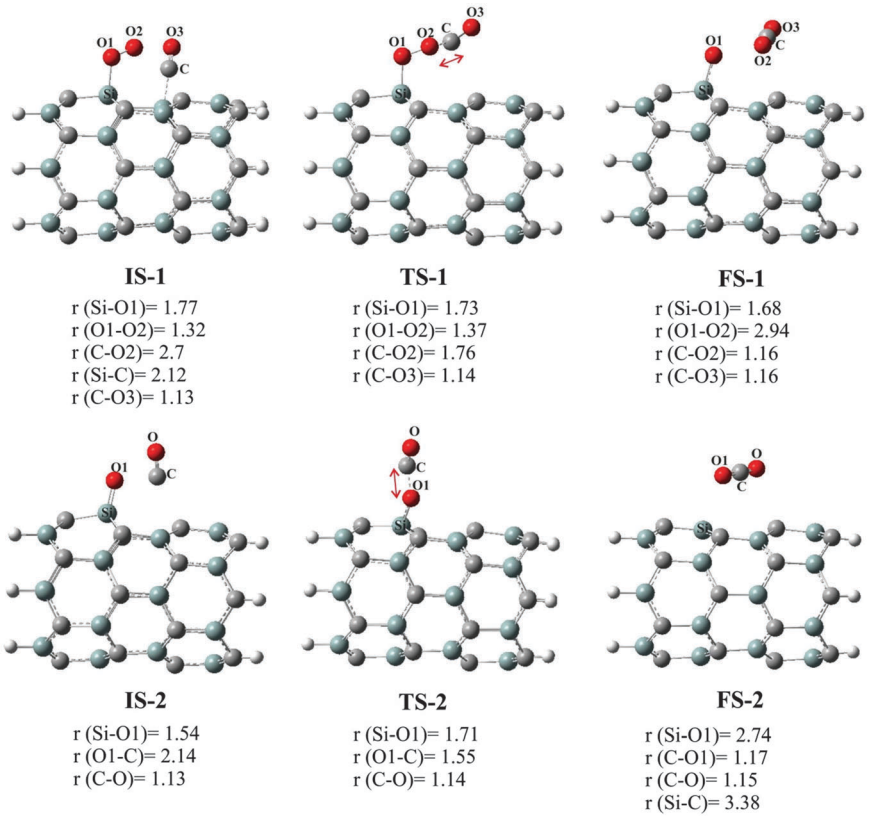

Fig. 5 Local configurations of the gas molecules over the (6,0) SiCNT in various states, including the initial state (IS), transition state (TS) and product (P) along the minimum-energy pathway *via* the $O_2 + CO \rightarrow O_{ads} + CO_2$ and $O_{ads} + CO \rightarrow CO_2$ routes. All bond distances are in Å.

In this structure, as is clear from Fig. 4, the CO molecule is in a vertical configuration more than 2.14 Å away from the O_{ads} atom pre-adsorbed on the SiCNT surface. The IS-2 can be converted to FS-2 through the transition state TS-2 with an energy barrier of 0.97 eV. The O–C–O complex in TS-2 is formed with Si–O_{ads} bond length of 1.71, in which the Si–O_{ads} is a little tilted towards the surface. Passing over the TS-2, the Si–O_{ads} bond length increases from 1.54 in IS-2 to 2.74 Å in the FS-2 state and the second CO_2 desorbs from the SiCNT surface. The process of IS-2 → FS-2 is exothermic with reaction energy of about −2.03 eV, which means that the O_{ads}–CO dissociation of CO_2 is irreversible at room temperature (Table 2).

In addition, the CO oxidation mechanism over the (5,0) SiCNT is investigated in detail. Fig. S5 of ESI,† demonstrates the energy profile of the CO oxidation reaction and the distinct geometric values are shown in Fig. S6 (ESI†). Moreover, the corresponding thermodynamic parameters are listed in Table S3 (ESI†). It should be noted that the triplet state of O_2 is considered during the investigation of CO oxidation over (5,0) SiCNT. As is clear, both the IS-3 → FS-3 and IS-4 → FS-4 pathways proceed *via* exothermic reactions (Table S3, ESI†), with activation energy of 0.89 and 1.79 eV, respectively. It can be concluded from the obtained results that the oxidation of a CO molecule occurs more easily over the (6,0) SiCNT than over the (5,0) SiCNT. This is most likely due to the weaker interaction of an O_2 molecule with the surface of the former nanotube, which reduces the activation energy for the CO oxidation reaction.

In this study, we completely described the CO oxidation over SiCNTs, because SiCNS shows similar catalytic activities to the tubular form. Thus, it is reasonable to assume that all the conclusions can also be applied to the SiCNS. The same as with a SiCNT, the CO oxidation reaction over a SiCNS begins with the LH mechanism and is followed by the ER, proceeding as: O_2–SiCNS + CO → O–SiCNS + CO_2 and O–SiCNS + CO → SiCNS + CO_2 reactions. The configurations for the IS, TS and FS along the reaction path are displayed in Fig. S7 (ESI†). In addition, the calculated activation energies and thermodynamic parameters are listed in Table 2. It was found that the oxidation of a CO molecule over the SiCNS is performed with lower energy barriers as compared with that over the SiCNT, therefore it can be considered as a more favorable catalyst for the oxidation of CO molecules.

4. Conclusion

Using DFT calculations, we explored the possibility of using a finite-sized zigzag SiCNT and SiC monolayer as a potential catalyst for CO oxidation by an O_2 molecule. For both SiCNT and SiCNS, the larger adsorption energy of O_2 compared to CO showed a great activity of O_2 for CO oxidation. Obtained results suggested that when a CO and O_2 mixture is injected as reaction gases, the Si-atoms of the SiCNT/SiCNS should be covered by the triplet O_2 molecules first and the CO molecule should be oxidized in the next steps. Moreover, it was found that the CO oxidation by O_2 over a (6,0) SiCNT (SiCNS) prefers to proceed *via* the LH mechanism with energy barrier of 0.86 (0.27) eV. The estimated activation energies on these metal-free catalysts are lower than those on the traditional noble metals. In addition, the adsorption energy of the O_2/CO molecule over the tube surface is increased with the reduction of tube diameter, whereas a reverse trend is evident for activation energies of CO oxidation. This is most likely due to the stronger interaction of O_2 and O_{ads} moieties with the surface of a (5,0) SiCNT, which increases the activation energy for the CO oxidation reaction. Therefore, it seems that large-diameter SiCNTs are more efficient for CO oxidation than small-diameter ones. Moreover, the change in length of the nanotube did not change the adsorption energies significantly. Considering the fact that the electronic structures of these nanotubes are almost independent of the tube chirality, it is obvious that the results of this study could be transferred to armchair or chiral SiCNTs. Moreover, it is suggested that due to the lower energy barrier of CO oxidation over SiCNSs, they may be considered as more favorable catalysts than SiCNTs for the oxidation of CO molecules. Thus, it is proposed that SiCNSs and SiCNTs can be considered as highly stable and highly active metal-free catalysts for CO oxidation.

References

1 A. A. Herzing, C. J. Kiely, A. F. Carley, P. Landon and G. J. Hutchings, *Science*, 2008, **321**, 1331–1335.
2 H. J. Freund, G. Meijer, M. Scheffler, R. Schlogl and M. Wolf, *Angew. Chem.*, 2011, **50**, 10064–10094.
3 X. Xie, Y. Li, Z. Q. Liu, M. Haruta and W. Shen, *Nature*, 2009, **458**, 746–749.
4 B. Qiao, A. Wang, X. Yang, L. F. Allard, Z. Jiang, Y. Cui, J. Liu, J. Li and T. Zhang, *Nat. Chem.*, 2011, **3**, 634–641.
5 S. Royer and D. Duprez, *ChemCatChem*, 2011, **3**, 24–65.
6 A. Hornés, A. Hungría, P. Bera, A. L. Cámara, M. Fernández-García, A. Martínez-Arias, L. Barrio, M. Estrella, G. Zhou and J. Fonseca, *J. Am. Chem. Soc.*, 2009, **132**, 34–35.
7 J. Zhang, H. Jin, M. B. Sullivan, F. C. H. Lim and P. Wu, *Phys. Chem. Chem. Phys.*, 2009, **11**, 1441–1446.
8 H.-Y. Su, M.-M. Yang, X.-H. Bao and W.-X. Li, *J. Phys. Chem. C*, 2008, **112**, 17303–17310.
9 S. Piccinin and M. Stamatakis, *ACS Catal.*, 2014, **4**, 2143–2152.
10 M. Chen, Y. Cai, Z. Yan, K. Gath, S. Axnanda and D. W. Goodman, *Surf. Sci.*, 2007, **601**, 5326–5331.
11 A. Alavi, P. Hu, T. Deutsch, P. L. Silvestrelli and J. Hutter, *Phys. Rev. Lett.*, 1998, **80**, 3650.
12 A. K. Geim and K. S. Novoselov, *Nat. Mater.*, 2007, **6**, 183–191.
13 F. Schedin, A. Geim, S. Morozov, E. Hill, P. Blake, M. Katsnelson and K. Novoselov, *Nat. Mater.*, 2007, **6**, 652–655.
14 M. D. Stoller, S. Park, Y. Zhu, J. An and R. S. Ruoff, *Nano Lett.*, 2008, **8**, 3498–3502.
15 A. C. Neto, F. Guinea, N. Peres, K. S. Novoselov and A. K. Geim, *Rev. Mod. Phys.*, 2009, **81**, 109.
16 P. V. Kamat, *J. Phys. Chem. Lett.*, 2009, **1**, 520–527.

17 C. O. Girit, J. C. Meyer, R. Erni, M. D. Rossell, C. Kisielowski, L. Yang, C. H. Park, M. F. Crommie, M. L. Cohen, S. G. Louie and A. Zettl, *Science*, 2009, **323**, 1705–1708.
18 Y. Shao, J. Wang, H. Wu, J. Liu, I. A. Aksay and Y. Lin, *Electroanalysis*, 2010, **22**, 1027–1036.
19 W. Choi, I. Lahiri, R. Seelaboyina and Y. S. Kang, *Crit. Rev. Solid State Mater. Sci.*, 2010, **35**, 52–71.
20 F. Li, J. Zhao and Z. Chen, *J. Phys. Chem. C*, 2012, **116**, 2507–2514.
21 Y. Shao, S. Zhang, M. H. Engelhard, G. Li, G. Shao, Y. Wang, J. Liu, I. A. Aksay and Y. Lin, *J. Mater. Chem.*, 2010, **20**, 7491.
22 J.-x. Zhao, Y. Chen and H.-g. Fu, *Theor. Chem. Acc.*, 2012, **131**, 1242.
23 F. Gao, G. L. Zhao, S. Yang and J. J. Spivey, *J. Am. Chem. Soc.*, 2013, **135**, 3315–3318.
24 M. Menon, E. Richter, A. Mavrandonakis, G. Froudakis and A. N. Andriotis, *Phys. Rev. B: Condens. Matter Mater. Phys.*, 2004, **69**, 115322.
25 G. L. Harris, *Properties of silicon carbide*, IET, 1995.
26 C. Virojanadara and L. Johansson, *Surf. Sci.*, 2002, **519**, 73–78.
27 H. Chang, J. Wu, B.-L. Gu, F. Liu and W. Duan, *Phys. Rev. Lett.*, 2005, **95**, 196803.
28 P. Zhang, B. B. Xiao, X. L. Hou, Y. F. Zhu and Q. Jiang, *Sci. Rep.*, 2014, **4**, 3821.
29 S. Lin, *J. Phys. Chem. C*, 2012, **116**, 3951–3955.
30 L. Wang, *Appl. Surf. Sci.*, 2012, **258**, 6688–6691.
31 P. Gori, O. Pulci, M. Marsili and F. Bechstedt, *Appl. Phys. Lett.*, 2012, **100**, 043110.
32 X.-H. Sun, C.-P. Li, W.-K. Wong, N.-B. Wong, C.-S. Lee, S.-T. Lee and B.-K. Teo, *J. Am. Chem. Soc.*, 2002, **124**, 14464–14471.
33 G. Gao and H. S. Kang, *J. Chem. Theory Comput.*, 2008, **4**, 1690–1697.
34 R. Wu, M. Yang, Y. Lu, Y. Feng, Z. Huang and Q. Wu, *J. Phys. Chem. C*, 2008, **112**, 15985–15988.
35 R. Moradian, S. Behzad and R. Chegel, *Physica B*, 2008, **403**, 3623–3626.
36 K. M. Alam and A. K. Ray, *Phys. Rev. B: Condens. Matter Mater. Phys.*, 2008, **77**, 035436.
37 M. D. Esrafili and H. Behzadi, *J. Mol. Model.*, 2013, **19**, 2375–2382.
38 M. D. Esrafili, V. Mokhtar Teymurian and R. Nurazar, *Surf. Sci.*, 2015, **632**, 118–125.
39 M. D. Esrafili and R. Nurazar, *J. Mol. Graphics Modell.*, 2015, **55**, 41–47.
40 M. D. Esrafili, R. Nurazar and V. Masumi, *Surf. Sci.*, 2015, **637**, 69–76.
41 M. J. Frisch, G. W. Trucks, H. B. Schlegel, G. E. Scuseria, M. A. Robb, *et al.*, *Gaussian 09, Revision D.01*, Gaussian, Inc., Wallingford, CT, 2009.
42 Y. Zhao and D. G. Truhlar, *Theor. Chem. Acc.*, 2008, **120**, 215–241.
43 M. D. Esrafili and R. Nurazar, *Superlattices Microstruct.*, 2014, **67**, 54–60.
44 M. Zhao, Y. Xia, R. Zhang and S.-T. Lee, *J. Chem. Phys.*, 2005, **122**, 214707.
45 J.-x. Zhao and Y.-h. Ding, *J. Chem. Theory Comput.*, 2009, **5**, 1099–1105.
46 X. Wang and K. M. Liew, *J. Phys. Chem. C*, 2011, **115**, 10388–10393.
47 K. Nakamura, T. Toriyama and S. Sugiyama, *Jpn. J. Appl. Phys.*, 2011, **50**, 06GE05.
48 H. Şahin, S. Cahangirov, M. Topsakal, E. Bekaroglu, E. Akturk, R. T. Senger and S. Ciraci, *Phys. Rev. B: Condens. Matter Mater. Phys.*, 2009, **80**, 155453.
49 B. Baumeier, P. Krüger and J. Pollmann, *Phys. Rev. B: Condens. Matter Mater. Phys.*, 2007, **76**, 085407.
50 E. H. Song, Z. Wen and Q. Jiang, *J. Phys. Chem. C*, 2011, **115**, 3678–3683.
51 S. Lin, X. Ye and J. Huang, *Phys. Chem. Chem. Phys.*, 2015, **17**, 888–895.
52 M. D. Esrafili, R. Mohammad-Valipour, S. M. Mousavi-Khoshdel and P. Nematollahi, *ChemPhysChem*, 2015, **16**, 3719–3727.
53 F. Cao, X. Xu, W. Ren and C. Zhao, *J. Phys. Chem. C*, 2009, **114**, 970–976.
54 Á. Szabó and A. Gali, *Phys. Rev. B: Condens. Matter Mater. Phys.*, 2009, **80**, 075425.
55 K. Li, W. Wang and D. Cao, *J. Phys. Chem. C*, 2011, **115**, 12015–12022.
56 J.-m. Jia, S.-p. Ju, D.-n. Shi and K.-f. Lin, *J. Nanopart. Res.*, 2013, **15**, 1977.
57 Y. Li, Z. Zhou, G. Yu, W. Chen and Z. Chen, *J. Phys. Chem. C*, 2010, **114**, 6250–6254.
58 S. Nigam and C. Majumder, *ACS Nano*, 2008, **2**, 1422–1428.
59 Y.-H. Lu, M. Zhou, C. Zhang and Y.-P. Feng, *J. Phys. Chem. C*, 2009, **113**, 20156–20160.
60 M. D. Esrafili and N. Saeidi, *Physica E*, 2015, **74**, 382–387.

